

Strain manipulation of Majorana fermions in graphene

Zhen-Hua Wang,¹ Eduardo V. Castro,² and Hai-Qing Lin¹

¹*Beijing Computational Science Research Center, Beijing 100084, China*

²*CeFEMA, Instituto Superior Técnico, Universidade de Lisboa, Av. Rovisco Pais, 1049-001 Lisboa, Portugal*

The functionalized graphene with induced superconductivity, Zeeman coupling, and finite Rashba spin-orbit coupling is proposed to display topological superconducting phases with Majorana end modes. We obtain the phase diagram of bulk graphene and nanoribbon by calculating the Chern number, band structure and wavefunction. The electron doping in graphene, magnetic field and strain-induced pseudomagnetic field can result in the topological phase transition. Moreover, it is interested to note that strain has negative influence on the stability of topological nontrivial phase either uniform or nonuniform, destroying the existence of Majorana fermion, which provides a new way to transfer, create and fuse Majorana fermions. Some experimental schemes are also introduced to tailor functionalized graphene, generating various devices applied in topological quantum computation.

PACS numbers: 73.63.Kv, 72.15.Qm, 73.63.Fg, 73.23.-b

I. INTRODUCTION

Graphene and related materials can be integrated with desired specific properties, in particular to the energy devices,^{1–5} topological quantum computations^{6–13} and wide spectrum of applications.^{14–20} With the development and optimization of production methods, high-volume liquid-phase exfoliation^{21–24} and chemical vapor deposition,^{25–27} functionalized graphene is tailored and exploited for various devices, such as portable and wearable energy conservation and shortage devices, water splitting, membranes, quantum walks and computation. Topological properties and the chiral symmetry inherent in graphene are the main reason why the seemingly simply honeycomb lattice accommodate such a rich physics,^{28–32} which includes double Dirac cones in the Brillouin zone,³³ anomalously sharp Landau level and quantum Hall effect at the Dirac point in magnetic field even with ripples, and a host of other peculiar features.^{34,35}

Graphene is one of the most promising nanomaterials because of its unique combination of superb properties. Experimental advances in doping methods have allowed the electron density to approach the van Hove singularities (VHSs) at 25% hole or electron doping.^{36,37} The logarithmically diverging density of states at the VHS can allow nontrivial ordered ground states to emerge due to strongly enhanced effects of interactions. Meanwhile, strain is used as a mechanism to change the energy of the VHS, bringing it closer to the doping level of pristine graphene, and therefore making it experimentally accessible. Topological insulators is predicted for graphene, where the weak intrinsic spin-orbit interaction (SOI) can be enhanced by applying a perpendicular electric field^{38,39} or a nonuniform magnetic field,⁴⁰ tuning the local curvature of the sheet,⁴¹ or doping by 3d or 5d transition metal adatoms.^{42–44} When graphene is deposited on substrates or adsorbed with heavy atoms, the interaction-induced symmetry breaking can open bulk gaps to support kinds of topological phases. Recently,

one common strategy to generate topological superconductor is through the coupling of an s-wave superconductor to the helical half-metallic graphene.^{45,46}

The exotic properties of graphene also led to an extensive study focusing on monolayer, bilayer, nanoribbon, and taking into account features such as strain and curvature, disorder, etc.^{47,48} Being able to influence the motion of charge carriers, strain-induced pseudomagnetic fields in graphene have been explored as a potential approach to engineering the electronic states of graphene.^{49,50} Nanoribbons also provide numerous interesting issues in fundamental physics, such as topological insulators.

The functionalized graphene in topological hybrid system has received less attention, and therefore graphene with induced superconductivity and Zeeman coupling, and finite Rashba spin-orbit coupling is proposed to display topological superconducting phases with Majorana end modes. Besides bulk graphene, nanoribbons are also designed to investigate their topological phase transition, and the uniform and nonuniform strain induced pseudomagnetic fields have great effect on the stability of topological nontrivial phase, which offer new method to transfer and control Majorana fermions (MF). Nonuniform chemical potential, Zeeman field and strain provide us enough quantum techniques to control functionalized graphene.

II. MODEL

In this work only nearest neighbor hopping processes are considered, shown in Fig. 1, the minimum tight binding model is used:

$$H_0 = -t \sum_{r,\sigma} a_{r,\sigma}^+ (b_{r,\sigma} + b_{r-a_1,\sigma} + b_{r-a_2,\sigma}) + h.c. - \mu \sum_{r,\sigma} (a_{r,\sigma}^+ a_{r,\sigma} + b_{r,\sigma}^+ b_{r,\sigma}), \quad (1)$$

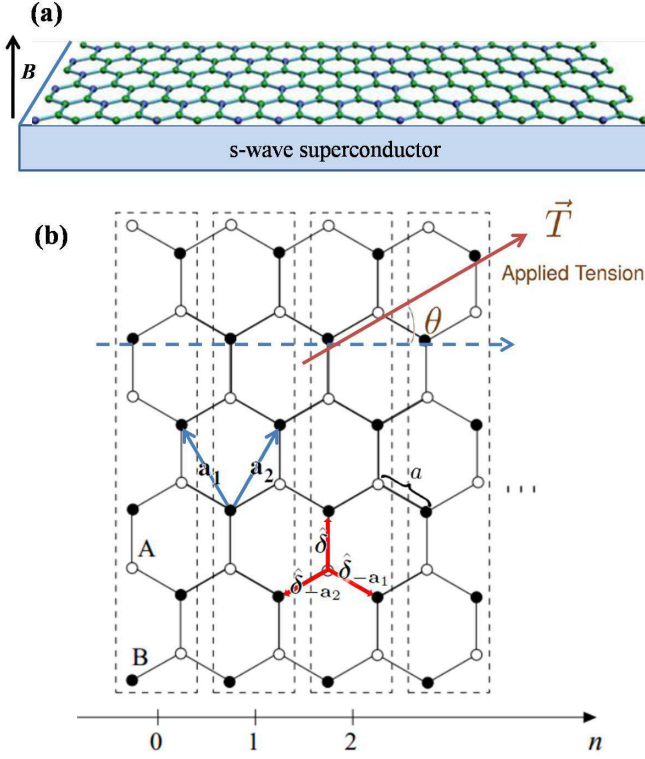


FIG. 1. Sketch of zigzag graphene nanoribbon. (a) The zigzag graphene nanoribbon on an s-wave superconductor, and the magnetic field B applied perpendicular to the surface can induce a topological regime, where bound states are formed inside the gap. (b) Honeycomb lattice geometry. The vectors $\hat{\delta}$, $\hat{\delta}_{-a_1}$ and $\hat{\delta}_{-a_2}$ connect A sites to their B site neighbors. The graphene ribbon is stretched or compressed along a prescribed direction, and θ is direction of applied tension T .

where r denotes the position on the Bravais lattice, and t connects the site r to its neighbors, μ is the chemical potential, and $a_{r,\sigma}$ ($b_{r,\sigma}$) annihilates an electron with spin σ on atom A (B) in the unit cell.

The Rashba SOI Hamiltonian is written as

$$H_R = i\lambda_R \sum_{r,\sigma,\sigma'} a_{r,\sigma}^+ [(\sigma \times \hat{\delta})_z^{\sigma\sigma'} b_{r,\sigma'} + (\sigma \times \hat{\delta}_{-a_1})_z^{\sigma\sigma'} b_{r-a_1,\sigma'} + (\sigma \times \hat{\delta}_{-a_2})_z^{\sigma\sigma'} b_{r-a_2,\sigma'}] + h.c., \quad (2)$$

where λ_R is strength of spin-orbit coupling, (σ, σ') stand for spin up and down.

The s-wave superconductivity is induced in the system by proximity effect and is described by a uniform on-site superconducting order parameter Δ whose Hamiltonian can be written as:

$$H_{SC} = \Delta \sum_r a_{r,\uparrow}^+ a_{r,\downarrow}^+ + b_{r,\uparrow}^+ b_{r,\downarrow}^+ + h.c.. \quad (3)$$

Finally, a magnetic field B is introduced, resulting in an out-of-plane Zeeman potential $V_Z = g\mu_B|B|/2$, with g the Landé g -factor and μ_B the Bohr magneton. This

Zeeman Hamiltonian is described as follows:

$$H_Z = V_Z \sum_{r,\sigma,\sigma'} (a_{r,\sigma}^+ \sigma_z^{\sigma\sigma'} a_{r,\sigma'} + b_{r,\sigma}^+ \sigma_z^{\sigma\sigma'} b_{r,\sigma'}). \quad (4)$$

We choose $a_{1(2)}$ as basis vectors in direct space

$$\mathbf{a}_{1(2)} = \sqrt{3}a(\mp \frac{1}{2}, \frac{\sqrt{3}}{2}), \quad (5)$$

and for the vectors connecting NN sites,

$$\begin{aligned} \hat{\delta} &= a(0, 1), \\ \hat{\delta}_{-a_1} &= a(\frac{\sqrt{3}}{2}, -\frac{1}{2}) \\ \hat{\delta}_{-a_2} &= a(-\frac{\sqrt{3}}{2}, -\frac{1}{2}). \end{aligned} \quad (6)$$

The basis vectors in reciprocal space may be chosen as,

$$\mathbf{b}_{1(2)} = \frac{4\pi}{3a}(\mp \frac{\sqrt{3}}{2}, \frac{1}{2}), \quad (7)$$

and the corners of the hexagonal Brillouin zone, where the gap closes, are given by

$$\pm \mathbf{K} = \pm \frac{\mathbf{b}_2 - \mathbf{b}_1}{3} = \frac{4\pi}{3a} \hat{e}_x. \quad (8)$$

We are also interested in uniform planar tension situations, where the graphene sheet is stretched or compressed uniformly along a prescribed direction. The fixed Cartesian system is chosen in a way that Ox always coincides with the zigzag direction of the lattice. The strain tensor in the lattice coordinate system reads:⁵¹

$$\vec{\varepsilon} = \varepsilon \begin{pmatrix} \cos^2 \theta - \sigma \sin^2 \theta & (1 + \sigma) \cos \theta \sin \theta \\ (1 + \sigma) \cos \theta \sin \theta & \sin^2 \theta - \sigma \cos^2 \theta \end{pmatrix}, \quad (9)$$

where ε is the tensile strain, and σ is the Poisson's ratio for graphene, $\sigma = 0.165$. θ is angle between the direction of strain $\vec{\varepsilon}$ and x direction. The modification of the atom distances distorts the reciprocal lattice as well, The primitive vectors of the reciprocal space changes according to

$$\begin{aligned} \mathbf{b}_1 &\simeq \frac{2\pi}{\sqrt{3}a}(-1 + \varepsilon_{11} - \frac{\varepsilon_{12}}{\sqrt{3}}, \frac{1}{\sqrt{3}} + \varepsilon_{12} - \frac{\varepsilon_{22}}{\sqrt{3}}), \\ \mathbf{b}_2 &\simeq \frac{2\pi}{\sqrt{3}a}(1 - \varepsilon_{11} - \frac{\varepsilon_{12}}{\sqrt{3}}, \frac{1}{\sqrt{3}} - \varepsilon_{12} - \frac{\varepsilon_{22}}{\sqrt{3}}), \end{aligned} \quad (10)$$

Let $\hat{\delta}$, $\hat{\delta}_{-a_1}$, and $\hat{\delta}_{-a_2}$ be the vectors connecting NN in the honeycomb,

$$t_{\hat{\delta}} = t(1 - \beta \varepsilon_{22})$$

$$t_{\hat{\delta}_{-a_1}} = t[1 - \beta(\frac{3}{4}\varepsilon_{11} - \frac{\sqrt{3}}{2}\varepsilon_{12} + \frac{1}{4}\varepsilon_{22})]$$

$$t_{\delta-a_2} = t[1 - \beta(\frac{3}{4}\varepsilon_{11} + \frac{\sqrt{3}}{2}\varepsilon_{12} + \frac{1}{4}\varepsilon_{22})], \quad (11)$$

where $\beta \approx -\partial \log t / \partial \log a \sim 2 - 3$.

The Rashba spin-orbit interaction in the strained honeycomb is

$$\lambda_{R_\delta} = t(1 + \beta'\varepsilon_{22})$$

$$\lambda_{R_{\delta-a_1}} = t[1 + \beta'(\frac{3}{4}\varepsilon_{11} - \frac{\sqrt{3}}{2}\varepsilon_{12} + \frac{1}{4}\varepsilon_{22})]$$

$$\lambda_{R_{\delta-a_2}} = t[1 + \beta'(\frac{3}{4}\varepsilon_{11} + \frac{\sqrt{3}}{2}\varepsilon_{12} + \frac{1}{4}\varepsilon_{22})]. \quad (12)$$

Here we assume $\beta = \beta'$.

III. RESULTS AND DISCUSSION

Graphene has been an extremely active subject of research in recent years. The main difference between the surface of a topological insulator and that of graphene is that the topological insulator has only one Dirac point (or valley) and no spin degeneracy, whereas graphene has two Dirac points and is spin degenerate.^{8,52} This difference has far-reaching consequences, including the possibility of generating new particles that have applications in quantum computing. Several ways have been put forward in the literature to discuss graphene's topological property, including breaking the symmetry of a graphene sheet by depositing it on a substrate, controlling its band structure by doping, and adjusting the electronic properties of a graphene bilayer by applying an external electric field perpendicular to the surface. Graphene is also amenable to other external influences, including mechanical deformation, which offers a tempting prospect of controlling graphene's properties by strain. Strain-induced pseudomagnetic fields in graphene have been explored as a potential approach to engineering the electronic states of graphene.^{49,50,53} In this work, we will investigate the topological phase in bulk graphene and finite nanoribbon, discussing the effect of strain.

A. Bulk phase diagram

Topological orders play a crucial role in the classification of various phases in low-dimensional systems, and the Chern number, due to the Berry potential induced in the Brillouin zone and characterize the integer quantum Hall effect (QHE), is one of the most typical topological invariant.⁵⁴ The gap-closing condition of H_{BDG} gives out possible topological phase transition points since the topological invariant cannot change without closing the

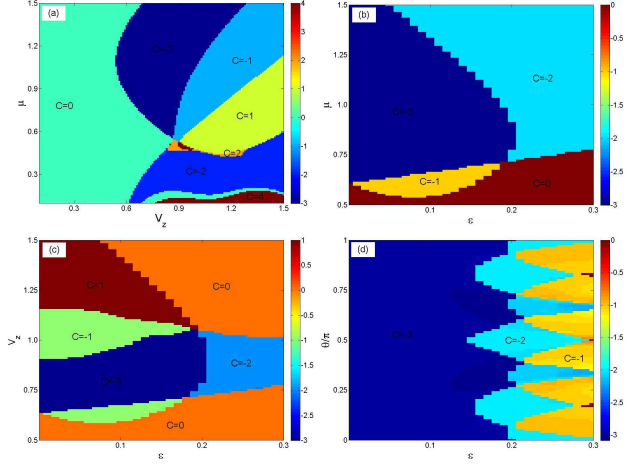


FIG. 2. The phase diagram of one layer graphene sheet obtained by Chern number. (a) Chern number as function of chemical potential μ and Zeeman field V_Z without strain. (b) Chern number vs μ and uniform strain ε , $V_Z = 0.8$, $\theta = 0$. (c) Chern number vs V_Z and uniform strain ε , $\mu = 0.8$, $\theta = 0$. (d) Chern number vs θ and uniform strain ε , $\mu = 0.8$, $V_Z = 0.8$. Other parameters: the nearest neighbor hopping without strain $t_0 = 1$, superconducting order $\Delta = 0.5$, Rashba SOI $\lambda_R = 0.2$, and $\sigma = 0.165$.

bulk energy gap. In Fig. 2, the quantum phase transition with Chern number of the bulk graphene electron system is established. When the pristine graphene with SOI couples to s-wave superconductor, this hybrid graphene system is always in insulating phase, $C = 0$. In Fig. 2(a), the magnetic field is switched on, perpendicular to the graphene surface, and the strong Zeeman field can induce the topological phase. When the Zeeman field $V_Z \leq 0.6$, the system is always in insulating phase $C = 0$. With the increase of V_Z , some other topological phases appear and the phase transition occurs. The odd Chern number corresponds to topological nontrivial phase, where the Majorana fermion is created, while the even Chern number corresponds to topological trivial phase. In Fig. 2(b)-(d), the strain-induced pseudomagnetic field can sharply change the topological property of graphene system. For low levels of electron doping, shown in Fig. 2(b), $\mu \leq 0.55$, the system is insulator even under strong magnetic and pseudomagnetic field. As $\mu \simeq 0.6$, the pseudomagnetic field induced by uniform strain along zigzag edge direction results in the topological phase transition, $C = 0 \rightarrow -1 \rightarrow 0$. With the increase of electron doping, the graphene transforms into topological nontrivial phase, $C = -3$. But uniform strain have negative influence on the stability of this nontrivial phase, where the larger the doping, the smaller the critical phase transition strain, ε_c . In Fig. 2(c), $\mu = 0.8$, corresponding size strain can help to induce nontrivial phase, in particular $\varepsilon \simeq 0.1$, a smaller magnetic field is enough to create topological nontrivial phase, $C = -1$. But if the Zeeman field is large enough, the critical ε_c

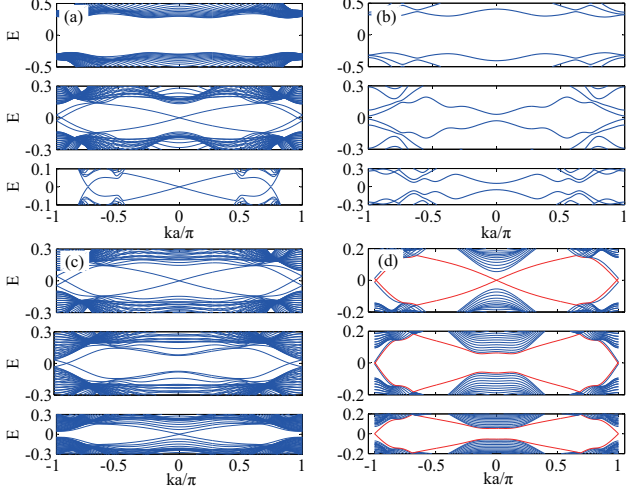


FIG. 3. The band structure of infinite zigzag nanoribbon. (a) The width of the ribbon is $W = 40$, and Zeeman field $V_Z = 0.3$ (Top), 0.8 (Middle), and 1.2 (Bottom), respectively. (b) The width of the ribbon is $W = 4$, and Zeeman field $V_Z = 0.3, 0.8$, and 1.2 , respectively. Other parameters: $t_0 = 1$, $\mu = 0.8$, $\Delta = 0.5$, $\lambda_R = 0.2$, $\theta = 0$, $\varepsilon = 0$ and $\sigma = 0.165$. (c)-(d) The band structure of different phases in the presence of strain. (c) (Top) $\mu = 0.8$, $V_Z = 0.8$, $\theta = 0$, $\varepsilon = 0.1$. (Middle) $\mu = 0.8$, $V_Z = 0.8$, $\theta = 0$, $\varepsilon = 0.25$. (Bottom) $\mu = 0.7$, $V_Z = 0.7$, $\theta = 0$, $\varepsilon = 0.1$. (d) (Top) $\mu = 0.8$, $V_Z = 0.8$, $\theta = 0.5\pi$, $\varepsilon = 0.1$. (Middle) $\mu = 0.8$, $V_Z = 0.8$, $\theta = 0.5\pi$, $\varepsilon = 0.2$. (Bottom) $\mu = 0.8$, $V_Z = 0.8$, $\theta = 0.4\pi$, $\varepsilon = 0.25$.

also decreases, similar to topological transport behavior as function of μ and ε . The main results in Fig. 2(d) present the influence of the direction of strain. Strong uniform strain can cause the system to be always in trivial phase when $\theta = 0$, but continuous phase transition occurs, $C = -3 \rightarrow -2 \rightarrow -1$, if the direction of the strain shifts away from zigzag edge. The reason may be the effective pseudomagnetic field along zigzag edge decreases. The obtained results indicate that the strain can be used as a potential way to control Majorana fermions.

Topological quantum numbers for the bulk can often be related with those for the edge states in finite systems.⁵⁵ With this bulk-edge correspondence topological properties which can be hidden in the bulk may thus become visible around the boundaries. The emergence of chiral edge states in the bulk gap is intimately related to the topological property of the bulk Bloch states in the valence bands. In Fig. 3, the band structure of infinite zigzag ribbon with width of forty unit cells ($W = 40$) in different topological phases are presented, which is characterized by different number of crossings at zero-energy. It is found that the number of gapless chiral edge states along the edge of the graphene ribbon equals to the the absolute value of Chern number. When the system is insulator, $C = 0$, a well defined gap exists, while $C = -3$ corresponds to three zero-energy crossings as well as one

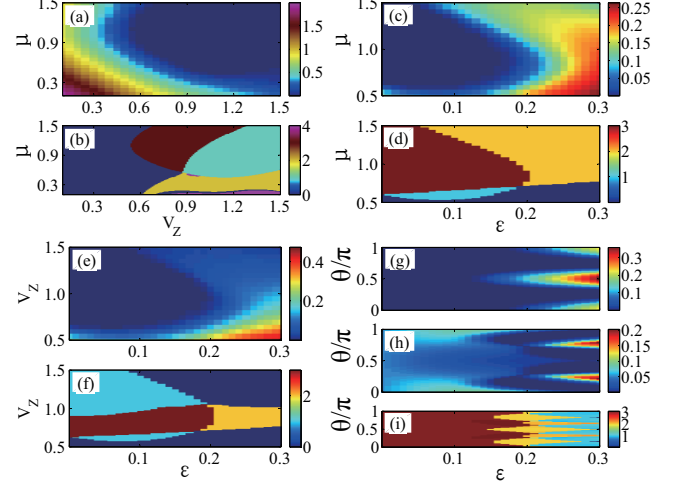


FIG. 4. The edge states of infinite zigzag nanoribbon with width of 40 unit cell ($W = 40$). (a), (c), (e), (g) The energy gap at $k = 0$, (h) the energy gap at $k = \pi$. (b), (d), (e), (i) The number of zero mode pairs is shown, odd number corresponds to topological nontrivial phase, even number is topological trivial phase and zero is insulating phase. Other parameters are the same as Fig. 2.

crossing for $C = -1$. In Fig. 3(b), the used parameters are the same as Fig. 3(a) except for the width of the ribbon, $W = 4$. It is noted that a finite gap between valence and conduction bands is always there. The reason is that the width of the ribbon is so narrow and the zigzag edge states can hybridize to each other. These results can also be verified by the eigenvalue calculation of finite nanoribbon with open boundary condition. It is also interested to note the difference of the zero-energy crossings between $\theta = 0$ and $\theta \neq 0$, shown in Fig. 3(d). When $\theta \neq 0$, the continuous phase transition occurs, $C = -3 \rightarrow -2 \rightarrow -1$, but the only one zero-energy state crosses at $k = \pi$ for $C = -1$. In Fig. 4, the band gap of infinite graphene zigzag nanoribbon with width of forty unit cells ($W = 40$) at $k = 0$ and π is calculated, as well as the number of gapless chiral edge states. In Fig. 4 (a), (c), (e), (g), the energy gap at $k = 0$ as function of μ , V_Z , θ , and ε presents two dispersive edge states crossing at zero energy if the system is in the topologically non-trivial phase. Fig. 3(h) shows the energy gap at $k = \pi$ as function of strain and its direction, it is found that the edge states crossing at $k = \pi$ as $\theta \neq n\pi$ ($n = 0, 1, 2, \dots$). In Fig. 4(b), (d), (f), (i), the number of gapless chiral edge states is counted, corresponding to the the absolute value of Chern number. The phase diagram obtained by Chern number is also demonstrated by band structure calculations.

B. Edge states in finite graphene nanoribbon

Designing graphene nanoribbons (GNRs) open the way to a breakthrough carbon-based electronics, in which the

lateral quantum confinement opens an electronic gap. Recent works have shown that a combination use of lithographic patterning of graphene samples and chemical methods such as solution-dispersion and sonication,⁵⁶ the designing GNRs can have narrow edges with controlled orientation, spatial localization, and electronic properties.⁴⁸ In this part, the investigation of the topological property and phase transition for narrow GNRs shows that the uniform strain-induced pseudomagnetic field have negative influence on the stability of topological nontrivial phase. In Fig. 5, a fixed size ribbon with length $L = 300$ and width $W = 4$ unit cells is chose to couple with s-wave superconductor, and its topological behavior is similar to a quasi-1D nanowire, where the zero-energy modes localize at the two ends of ribbon. A spinless quantum dot coupled to ribbon end is used as scanning tunneling microscope (STM) to verify the topological phase transition. Universal zero-bias anomalies provides a powerful method to infer the existence of Majorana mode, in particular, it is in the topological nontrivial phase, $G_{peak} = 1/2$ (e^2/h), in contrast to that for a dot coupled to a regular fermionic zero mode, $G_{peak} = 0$, and its topologically trivial phase, $G_{peak} = 1$.^{57,58} In Fig. 5(a), the appearance of Majorana zero mode required high level of electron doping and strong magnetic field. Upon increasing the Zeeman field, the ribbon undergoes a series of topological quantum phase transition as it traverses successive topological trivial and nontrivial phases. Fig. 5(b) presents the combination effect of electron doping and uniform strain affects the stability of Majorana zero mode, where strong strain destroys the topological nontrivial phase at small μ , but it nearly has no influence on the nontrivial phase stability at high μ . The magnetic field and strain-induced pseudomagnetic field would have opposing effect, shown in Fig. 5(c). At moderate magnetic field, strong strain induces the topological phase transition from nontrivial to trivial phase, and successive phase transition undergoes at strong magnetic field. Fig. 5(d) indicates that the effective pseudomagnetic field along zigzag edge changes with the direction of the strain, and strain along armchair direction can have sharply effect, requiring small critical strain ε_c .

Recently, a local Majorana polarization is also used as order parameters to characterize the topological transition between the trivial and nontrivial system.⁵⁹ For a given eigenstate, $\Psi^+ = (u_\uparrow, u_\downarrow, \nu_\uparrow, \nu_\downarrow)$, with u and ν respectively the electron and hole amplitudes, the Majorana polarizations along the x - and y -axis are defined as:

$$\begin{aligned} P_{M_x} &= 2\text{Re}[u_\downarrow \nu_\downarrow^* - u_\uparrow \nu_\uparrow^*], \\ P_{M_y} &= 2\text{Im}[u_\downarrow \nu_\downarrow^* - u_\uparrow \nu_\uparrow^*]. \end{aligned} \quad (13)$$

The Majorana polarization P_{M_x} and P_{M_y} for the lowest energy states ($n = \pm 1$) are plotted in Fig. 6. When there is no strain on the symmetry zigzag ribbon, shown in Fig. 6(a), the system is in topological nontrivial phase, and the values of the Majorana polarization P_{M_x} are always opposite at the two ends of the ribbon, while P_{M_y}

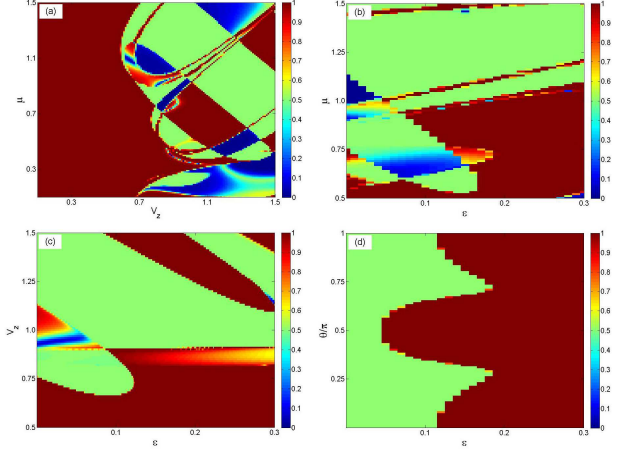


FIG. 5. The pronounced zero-bias peak of detecting quantum dot is used to verify the phase of finite nanoribbon, $A(\omega) = -2\text{Im}(G_{1\downarrow}^R(\omega) + G_{2\downarrow}^R(\omega))$. Only the spin-down channel is considered because of the large Zeeman splitting. (a) $\theta = 0$, $\varepsilon = 0.0$. (b) $\theta = 0$, $V_Z = 0.8$. (c) $\theta = 0$, $\mu = 0.8$. (d) $\mu = 0.8$, $V_Z = 0.8$. Other parameters: $t_0 = 1$, $\Delta = 0.5$, $\lambda_R = 0.2$, and $\sigma = 0.165$.

are always equal at two ends. In Fig. 6(b), the uniform strain $\varepsilon = 0.1$ along zigzag edge is switched on, the ribbon is always in its topological nontrivial phase, and the opposite P_{M_x} at two ends is preserved, P_{M_y} are always equal. The main difference between no strain case is that the Majorana polarization becomes delocalized. In Fig. 6(c), $\varepsilon = 0.25$, the ribbon is in topological trivial phase, P_{M_x} and P_{M_y} are nearly zero in all sites of the ribbon. Therefore, Majorana polarization is also a good order parameter to characterize the topological transition. In Fig. 6(d)-(e), non-uniform strain is applied along zigzag direction, and the strain increases as an arithmetic series along x direction, $\varepsilon_{\max} = 0.05$ and 0.15 , respectively. It is found that P_{M_x} are always opposite but with different strength at the two ends of the ribbon, and P_{M_y} are unequal. As $\varepsilon_{\max} = 0.15$, the topological nontrivial phase will disappear in high strain region and topological nontrivial phase edge starts to move away from high strain. In Fig. 6(f), the other kind of non-uniform strain is applied,

$$\varepsilon = \varepsilon_{\max} \frac{1}{2} [1 + \tanh(\frac{x - x_0}{\zeta})], \quad (14)$$

where ε_{\max} is maximum strain at right end, x is sites of the ribbon, x_0 is the sites with maximum slope, and ζ can control the slope of the line. It is also observed that the non-uniform strain can move the Majorana polarization. For armchair graphene nanoribbon, the values of the Majorana polarization P_{M_y} are always opposite at the two ends of the ribbon, and P_{M_x} are always equal at two ends. In non-uniform graphene nanoribbon, the symmetry of the Majorana polarization is destroyed. According to the calculation, it conforms that a MF is always spin

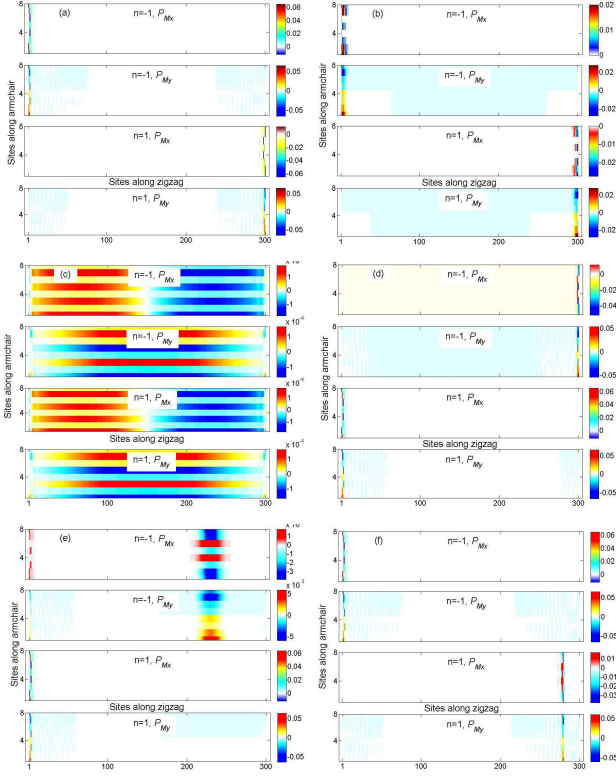


FIG. 6. The Majorana polarization of two zero-modes inside the gap. Majorana polarization is also a good order parameter to characterize the topological transition. (a) Uniform strain along zigzag edge $\varepsilon = 0$. (b) $\varepsilon = 0.1$. (c) $\varepsilon = 0.25$. (d) Non-uniform strain, the strain increases as an arithmetic series, $\varepsilon_{\max} = 0.05$. (e) $\varepsilon_{\max} = 0.15$. (f) Non-uniform strain distributes as function \tanh . Other parameters: $t_0 = 1$, $\mu = 0.8$, $V_Z = 0.8$, $\Delta = 0.5$, $\lambda_R = 0.2$, $\theta = 0$, and $\sigma = 0.165$.

polarized in the sense that for a given tunnel junction, there exist a spin-quantization axis along which it is only possible to tunnel into or out of the state with electrons with a specific spin projection.

In Fig. 7, the Majorana polarization P_{M_x} and P_{M_y} for the lowest energy states as function of uniform strain ε are plotted, where $\mu = V_Z = 0.8$. Fig. 7(a) gives the energy values for different strain indicating the phase transition point at the uniform strain $\varepsilon \geq 0.115$. This phase transition behavior can also be observed from Majorana polarization, shown in Fig. 7(b)-(c), the values of the Majorana polarization P_{M_x} are always opposite at the two ends of the ribbon as the ribbon is in its topological nontrivial phase, while P_{M_y} are always equal at two ends. When the system is in trivial phase, there is no Majorana polarization. In Fig. 7(d), the pronounced zero-bias peak of coupled spinless quantum dot also gives the critical strain value $\varepsilon_c = 0.115$ where topological phase transition occurs. Therefore, for narrow GNRs, the uniform strain can also be applied to control the creation and transfer of Majorana zero modes.

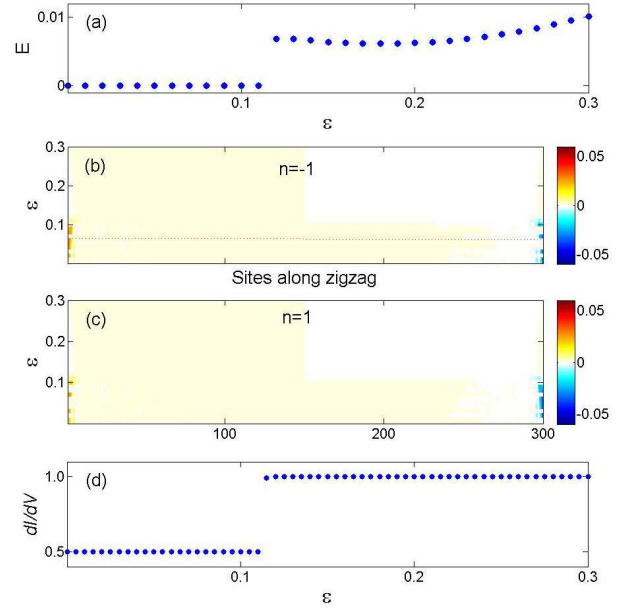


FIG. 7. The topological phase transition characterized by Majorana polarization P_{M_x} . (a) The lowest energy ($n=1$) as function of uniform strain. (b)-(c) Majorana polarization P_{M_x} vs uniform strain. (d) The phase transition characterized by the pronounced zero-bias peak of detecting quantum dot. $\varepsilon_c = 0.115$ is critical strain value where topological phase transition occurs. Other parameters: $t_0 = 1$, $\mu = 0.8$, $V_Z = 0.8$, $\Delta = 0.5$, $\lambda_R = 0.2$, $\theta = 0$, and $\sigma = 0.165$.

Graphene nanoribbon exhibits band gap modulation when subjected to strain. Besides uniform strain, nano-engineered non-uniform strain distribution in graphene is also a promising road to generate a band gap and a large pseudomagnetic field.^{60,61} Mechanical deformations such as nanoribbon twist, bending and inhomogeneous deformation can lead to non-uniform strain.⁶² Recent experiments showed that non-uniform strain can also be produced by depositing graphene over pillars. Here, we consider two types of non-uniform strain with different distribution rule, linear and nonlinear. Firstly, we consider the case that the strain increases as an arithmetic series along x direction, and the maximum strain localizes at right end of the ribbon. The main results are present in Fig. 8. At the left end of the ribbon, the strain is small and the left MF always localizes at it, but the right end has large strain and the localization of right MF is changed. So we only plot the wavefunction of right MF. In Fig. 8(a), as the $\varepsilon_{\max} = 0.1$, the wavefunction of right MF becomes delocalized. When the maximum strain ε_{\max} is large than 0.115, shown in Fig. 8(b)-(d), the wavefunction becomes more delocalization and move to low strain region. The obtained critical strain value ε_c of phase transition is the same as uniform strain. Therefore, both the uniform and non-uniform strain can provide a new way to manipulate Majorana fermions.

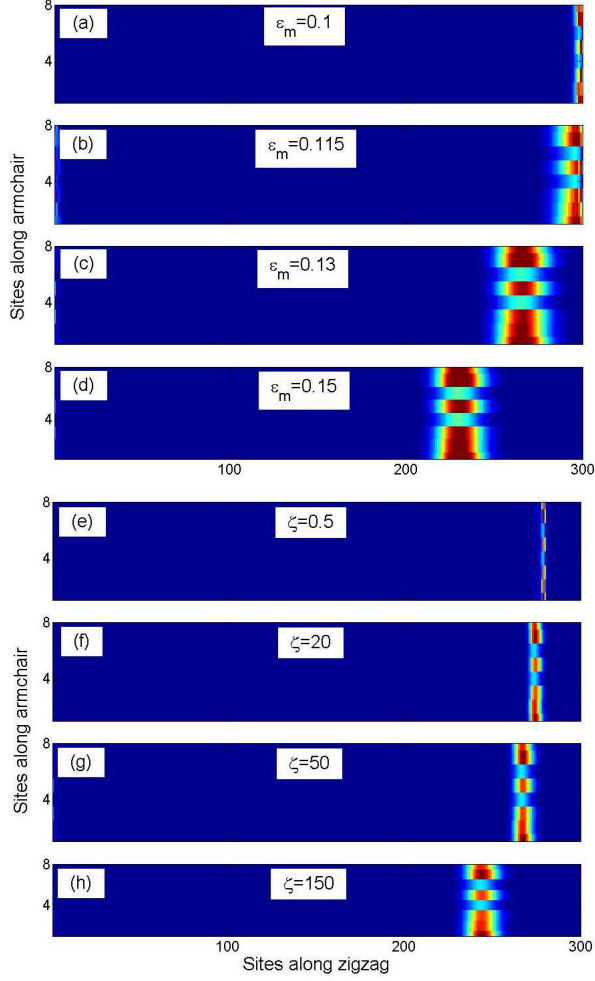


FIG. 8. The critical value of strain. (a)-(d) The strain increases as an arithmetic series. (a) $\varepsilon_{\max} = 0.1$. (b) $\varepsilon_{\max} = 0.115$. (c) $\varepsilon_{\max} = 0.13$. (d) $\varepsilon_{\max} = 0.15$. (e)-(h) The non-uniform strain is distributed as tanh function, and $\varepsilon_c = 0.115$. If the strain of one region exceeds ε_c , the region will be into non-topological region. (e) $\zeta = 0.5$, (f) $\zeta = 20$, (g) $\zeta = 50$, and (h) $\zeta = 150$. Other parameters: $t_0 = 1$, $\mu = 0.8$, $V_Z = 0.8$, $\Delta = 0.5$, $\lambda_R = 0.2$, $\theta = 0$, and $\sigma = 0.165$.

To get a deep insight into the non-uniform strain-induced pseudomagnetic field, the strain is distributed nonlinear, as in Eq. (14). When $\zeta \ll Na$, the strain will have a sharp increase at $x = x_0$, and becomes smooth on other sites. As can be seen from Fig. 8(e)-(h), $\varepsilon_{\max} = 0.3$ and $x_0 = 280$, the smaller the ζ , the larger the slope at x_0 . When $\zeta = 0.5$, the right MF localizes at $x = 279$, and the high strain region becomes non topological region, this behavior indicates that the pseudomagnetic field induced by large strain is harmful to the stability of topological non-trivial phase. In Fig. 8(f)-(h), $\zeta = 20, 50, 150$, respectively, the strain starts to spread over the whole ribbon, and the right MF transfers to left end, localizing at $x = 275, 268, 244$. The critical strain is $\varepsilon_c = 0.115$,

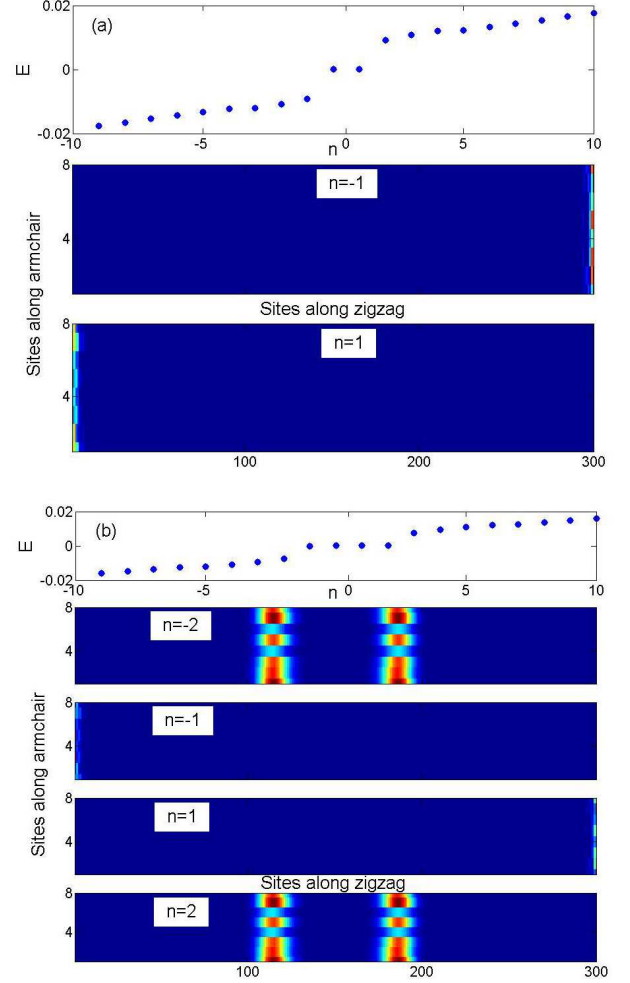


FIG. 9. Non-uniform strain creates new Majorana fermions. The maximum strain localizes at the middle of the ribbon. (a) $\varepsilon_{\max} = 0.1$. (b) $\varepsilon_{\max} = 0.15$. The other parameters are the same as Fig. 8.

where the right MF localizes. At the same time, the right MF becomes delocalized. As the distance between two MFs is much small, the wavefunction of the two MFs become overlap, and the system transfers to topological trivial phase. When the maximum strain $\varepsilon_{\max} \leq \varepsilon_c$, the two MF will always localize at the two ends of the ribbon, and the whole ribbon is in the topological nontrivial phase.

Furthermore, the strain distribution can be non-monotone variation, such as bending ribbon. It is therefore interesting to study the case that the strain linearly increases at first and then decreases to zero. In Fig. 9(a), the maximum strain at the middle of the ribbon is $\varepsilon_{\max} = 0.1 < \varepsilon_c = 0.115$, the whole ribbon is always in its topological nontrivial phase. But as $\varepsilon_{\max} = 0.15 > \varepsilon_c$, there is a new window opens in the middle region of the ribbon, $\varepsilon > \varepsilon_c$, which is trivial phase. Meanwhile, there

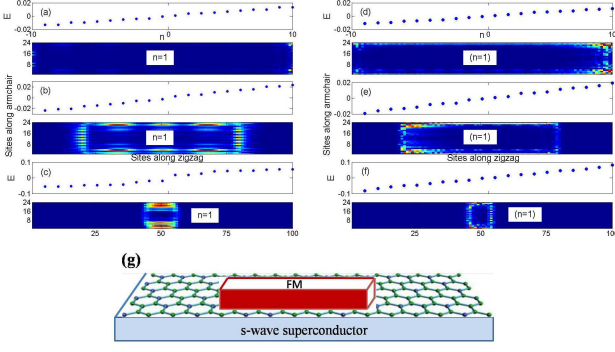


FIG. 10. The Majorana fermions in the wide ribbon. Non-uniform chemical potential helps to move topological region. The width is $W = 12$ unit cell, the length is 100 unit cell. (a) $l = 100$. (b) $l = 60$. (c) $l = 10$. Other parameters: $t_0 = 1$, $V_Z = 0.7$, $\Delta = 0.5$, $\lambda_R = 0.2$, $\theta = 0$, $\varepsilon = 0$ and $\sigma = 0.165$.

are two topological nontrivial regions in the ribbon, separating by a domain wall induced by the maximum strain at the middle of the ribbon. For this reason, there are two pairs zero-energy modes inside the gap, and the non-uniform strain creates a new pair of Majorana fermions instead of local gate.

C. Experimental realization

As discussed above, designing graphene nanoribbons have been put forward theoretically and experimentally. Next, we propose some alternative devices without strain to form the nanoribbon boundaries in graphene sheet by use of quantum control techniques. Here we choose a finite ribbon, with width $W = 12$ and length $L = 100$ unit cells, as the target systems. In Fig. 10(a)-(c), using the local gate, the non-uniform chemical potential is distributed as

$$u = u_c - \delta \left[1 - \tanh\left(\frac{x - (x_0 - l/2)}{\zeta}\right) \tanh\left(\frac{-x + (x_0 - l/2)}{\zeta}\right) \right], \quad (15)$$

where u_c is critical value to achieve topological nontrivial phase, x is sites of the ribbon, x_0 is the sites with maximum slope, ζ can control the slope of the line, δ is the gap away from u_c , l is the length of topological nontrivial

region. When the ribbon has large length and width, but length is much large than width, the system looks like a infinite nanoribbon and the Majorana zero-energy states localize at the edges of the ribbon. If the width is very narrow, the ribbon is similar to a nanowire and the Majorana end states localize at the two end of the ribbon. Fig. 10 gives comparable width to the length of finite ribbon, and the zero-energy states localize around the four edges, forming a rectangle region. From Fig. 10(a)-(c), the rectangle's area decreases with l , suggesting the non-uniform potential defined topological nontrivial region. In Fig. 10(d)-(f), non-uniform Zeeman field is introduced to control the topological nontrivial area, depending on the size of ferromagnetic, as the sketch in Fig. 10(g). The magnetic field is written as

$$V_z = \frac{(V_z)_c}{2} \left[1 - \tanh\left(\frac{x - (x_0 - l/2)}{\zeta}\right) \tanh\left(\frac{-x + (x_0 - l/2)}{\zeta}\right) \right], \quad (16)$$

where $(V_z)_c$ is critical value to achieve topological nontrivial phase. Similar results are obtained to non-uniform chemical potential.

IV. CONCLUSION

In this work, the topological phase transition in bulk graphene and nanoribbon are discussed in detail by calculating the Chern number, band structure and wavefunction. The Majorana fermions in bulk graphene and finite nanoribbon localize at different position, where the topological property hidden in the bulk becomes visible around boundaries, and MF wavefunction of narrow ribbon localizes at the two ends. According to the calculation of strain-induced pseudomagnetic field, it is observed that strain has negative influence on the stability of topological nontrivial phase either uniform or nonuniform. This special property provides a new way to transfer, create and fuse Majorana fermions, which is useful in designing topological quantum computation. For experimental realization, the nonuniform chemical potential, Zeeman field and strain can be used as quantum control techniques to form ribbon of arbitrary shape, tailoring functionalized graphene.

ACKNOWLEDGEMENT

¹ F. Bonaccorso, L. Colombo, G. Yu, M. Stoller, V. Tozzini, A. C. Ferrari, R. S. Ruoff, and V. Pellegrini, *Science* **347**, 1246501 (2015).
² D. Berman, S. A. Deshmukh, S. K. Sankaranarayanan, A. Erdemir, and A. V. Sumant, *Science*, 1262024 (2015).
³ X. Fan, Z. Peng, R. Ye, H. Zhou, and X. Guo, *ACS nano* **9**, 7407 (2015).

⁴ V. Skrypnichuk, N. Boulanger, V. Yu, M. Hilke, S. C. Mannsfeld, M. F. Toney, and D. R. Barbero, *Adv. Funct. Mater.* **25**, 664 (2015).
⁵ V. Georgakilas, M. Otyepka, A. B. Bourlinos, V. Chandra, N. Kim, K. C. Kemp, P. Hobza, R. Zboril, and K. S. Kim, *Chem. Rev.* **112**, 6156 (2012).
⁶ I. G. Karafyllidis, *J. Comput. Sci.* (2015).

- ⁷ M. Z. Hasan and C. L. Kane, *Rev. Mod. Phys.* **82**, 3045 (2010).
- ⁸ J. E. Moore, *Nature* **464**, 194 (2010).
- ⁹ X. Du, I. Skachko, F. Duerr, A. Luican, and E. Y. Andrei, *Nature* **462**, 192 (2009).
- ¹⁰ K. I. Bolotin, F. Ghahari, M. D. Shulman, H. L. Stormer, and P. Kim, *Nature* **462**, 196 (2009).
- ¹¹ A. Stern and N. H. Lindner, *Science* **339**, 1179 (2013).
- ¹² G.-P. Guo, Z.-R. Lin, T. Tu, G. Cao, X.-P. Li, and G.-C. Guo, *New J. Phys.* **11**, 123005 (2009).
- ¹³ L. Kou, B. Yan, F. Hu, S.-C. Wu, T. O. Wehling, C. Felser, C. Chen, and T. Frauenheim, *Nano Lett.* **13**, 6251 (2013).
- ¹⁴ Q. He, H. G. Sudibya, Z. Yin, S. Wu, H. Li, F. Boey, W. Huang, P. Chen, and H. Zhang, *Acs Nano* **4**, 3201 (2010).
- ¹⁵ T. Premkumar and K. E. Geckeler, *Prog. Polym. Sci.* **37**, 515 (2012).
- ¹⁶ M. S. Artiles, C. S. Rout, and T. S. Fisher, *Adv. Drug Deliv. Rev.* **63**, 1352 (2011).
- ¹⁷ N. Mohanty and V. Berry, *Nano Lett.* **8**, 4469 (2008).
- ¹⁸ V. Singh, D. Joung, L. Zhai, S. Das, S. I. Khondaker, and S. Seal, *Prog. Mater. Sci.* **56**, 1178 (2011).
- ¹⁹ X. Huang, Z. Zeng, Z. Fan, J. Liu, and H. Zhang, *Adv. Mater.* **24**, 5979 (2012).
- ²⁰ A. L. Ivanovskii, *Russ. Chem. Rev.* **81**, 571 (2012).
- ²¹ Y. Hernandez, V. Nicolosi, M. Lotya, F. M. Blighe, Z. Sun, S. De, I. McGovern, B. Holland, M. Byrne, Y. K. Gun'Ko, *et al.*, *Nat. Nanotechnol.* **3**, 563 (2008).
- ²² S. Park and R. S. Ruoff, *Nat. Nanotechnol.* **4**, 217 (2009).
- ²³ D. Wei, L. Grande, V. Chundi, R. White, C. Bower, P. Andrew, and T. Ryhänen, *Chem. Commun.* **48**, 1239 (2012).
- ²⁴ K. R. Paton, E. Varrla, C. Backes, R. J. Smith, U. Khan, A. O'Neill, C. Boland, M. Lotya, O. M. Istrate, P. King, *et al.*, *Nat. Mater.* **13**, 624 (2014).
- ²⁵ R. Raccichini, A. Varzi, S. Passerini, and B. Scrosati, *Nat. Mater.* **14**, 271 (2015).
- ²⁶ M. J. Allen, V. C. Tung, and R. B. Kaner, *Chem. Rev.* **110**, 132 (2009).
- ²⁷ A. Ismach, C. Druzgalski, S. Penwell, A. Schwartzberg, M. Zheng, A. Javey, J. Bokor, and Y. Zhang, *Nano Lett.* **10**, 1542 (2010).
- ²⁸ Y. Hatsugai and H. Aoki, in *Physics of Graphene* (Springer, 2014) pp. 213–250.
- ²⁹ K. Novoselov, A. K. Geim, S. Morozov, D. Jiang, M. Katsnelson, I. Grigorieva, S. Dubonos, and A. Firsov, *Nature* **438**, 197 (2005).
- ³⁰ A. K. Geim and K. S. Novoselov, *Nat. Mater.* **6**, 183 (2007).
- ³¹ Y. Zhang, Y.-W. Tan, H. L. Stormer, and P. Kim, *Nature* **438**, 201 (2005).
- ³² P. Bhattacharya, R. Fornari, and H. Kamimura, *Comprehensive Semiconductor Science and Technology, Six-Volume Set: Online version*, Vol. 1 (Newnes, 2011) pp. 179–205.
- ³³ W. Lomer, in *Proceedings of the Royal Society of London A: Mathematical, Physical and Engineering Sciences*, Vol. 227 (The Royal Society, 1955) pp. 330–349.
- ³⁴ Y. Hatsugai, *Solid State Commun.* **149**, 1061 (2009).
- ³⁵ Y. Hatsugai, *J. Phys. Soc. Jpn.* **75**, 123601 (2006).
- ³⁶ X. Chen, Y. Yao, H. Yao, F. Yang, and J. Ni, *Phys. Rev. B* **92**, 174503 (2015).
- ³⁷ A. M. Black-Schaffer, *Phys. Rev. Lett.* **109**, 197001 (2012).
- ³⁸ D. K. Efetov and P. Kim, *Phys. Rev. Lett.* **105**, 256805 (2010).
- ³⁹ M. Zarea and N. Sandler, *Phys. Rev. B* **79**, 165442 (2009).
- ⁴⁰ J. Klinovaja and D. Loss, *Phys. Rev. X* **3**, 011008 (2013).
- ⁴¹ D. Huertas-Hernando, F. Guinea, and A. Brataas, *Phys. Rev. B* **74**, 155426 (2006).
- ⁴² J. L. McClesney, A. Bostwick, T. Ohta, T. Seyller, K. Horn, J. González, and E. Rotenberg, *Phys. Rev. Lett.* **104**, 136803 (2010).
- ⁴³ O. Shevtsov, P. Carmier, C. Groth, X. Waintal, and D. Carpentier, *Phys. Rev. B* **85**, 245441 (2012).
- ⁴⁴ J. Hu, J. Alicea, R. Wu, and M. Franz, *Phys. Rev. Lett.* **109**, 266801 (2012).
- ⁴⁵ J. Alicea, *Rep. Prog. Phys.* **75**, 076501 (2012).
- ⁴⁶ P. San-Jose, J. L. Lado, R. Aguado, F. Guinea, and J. Fernández-Rossier, *Phys. Rev. X* **5**, 041042 (2015).
- ⁴⁷ J. Klinovaja, G. J. Ferreira, and D. Loss, *Phys. Rev. B* **86**, 235416 (2012).
- ⁴⁸ T. Wassmann, A. P. Seitonen, A. M. Saitta, M. Lazzeri, and F. Mauri, *Phys. Rev. Lett.* **101**, 096402 (2008).
- ⁴⁹ F. Guinea, M. Katsnelson, and A. Geim, *Nat. Phys.* **6**, 30 (2010).
- ⁵⁰ S. Zhu, J. A. Stroscio, and T. Li, *Phys. Rev. Lett.* **115**, 245501 (2015).
- ⁵¹ V. M. Pereira, A. H. Castro Neto, and N. M. R. Peres, *Phys. Rev. B* **80**, 045401 (2009).
- ⁵² A. H. Castro Neto, F. Guinea, N. M. R. Peres, K. S. Novoselov, and A. K. Geim, *Rev. Mod. Phys.* **81**, 109 (2009).
- ⁵³ T. M. G. Mohiuddin, A. Lombardo, R. R. Nair, A. Bonetti, G. Savini, R. Jalil, N. Bonini, D. M. Basko, C. Galiotis, N. Marzari, K. S. Novoselov, A. K. Geim, and A. C. Ferrari, *Phys. Rev. B* **79**, 205433 (2009).
- ⁵⁴ T. Fukui and Y. Hatsugai, *Phys. Rev. B* **75**, 121403 (2007).
- ⁵⁵ Y. Hatsugai, T. Fukui, and H. Aoki, *Phys. Rev. B* **74**, 205414 (2006).
- ⁵⁶ M. Y. Han, B. Özyilmaz, Y. Zhang, and P. Kim, *Phys. Rev. Lett.* **98**, 206805 (2007).
- ⁵⁷ D. E. Liu and H. U. Baranger, *Phys. Rev. B* **84**, 201308 (2011).
- ⁵⁸ Z.-H. Wang, X.-Y. Kuang, M.-M. Zhong, Z.-X. Yang, and H. Li, *EPL (Europhys. Lett.)* **106**, 67008 (2014).
- ⁵⁹ D. Sticlet, C. Bena, and P. Simon, *Phys. Rev. Lett.* **108**, 096802 (2012).
- ⁶⁰ M. Neek-Amal, L. Covaci, and F. M. Peeters, *Phys. Rev. B* **86**, 041405 (2012).
- ⁶¹ H. Tomori, A. Kanda, H. Goto, Y. Ootuka, K. Tsukagoshi, S. Moriyama, E. Watanabe, and D. Tsuya, *Appl. Phys. Express* **4**, 075102 (2011).
- ⁶² A. Dobrinsky, A. Sadrzadeh, B. Yakobson, and J. Xu, *Int. J. High Speed Electron. Syst.* **20**, 153 (2011).